Influence of PM Coating on PM Magnetization State Estimation Methods Based on Magnetoresistive Effect

Daniel Fernandez[1], David Reigosa[1], Juan Manuel Guerrero[1], Zi-Qiang Zhu[2], Fernando Briz[1]
[1]University of Oviedo. Dept. of Elect., Computer & System Engineering, Gijón, 33204, Spain.
[2] University of Sheffield. Department of Electronic and Electrical Engineering, UK.
fernandezalodaniel@uniovi.es, diazdavid@uniovi.es, guerrero@uniovi.es, z.q.zhu@sheffield.ac.uk, fernando@isa.uniovi.es

***Abstract*—Variable flux PMSMs (VF-PMSMs) are gaining importance, especially in automotive applications. The use of such machines will require the development of methods to estimate the permanent magnet (PM) magnetization state. PM magnetization state estimation methods reported in literature include BEMF and high frequency signal injection. One advantage of high frequency signal injection methods is that they can operate over the whole speed range, with practically no interference with the regular operation of the machine. Magnetization estimation using high frequency injection relies on the variation of the *d*-axis high frequency inductance with the saturation produced by the magnets. Alternatively, the changes of the magnet electrical resistance due to the magnetoresistive effect can also be used for this purpose. These methods have been tested with different materials, including NdFeB, AlNiCo and SmCo magnets. NdFeB magnets are usually protected from oxidation using NiCuNi coating. However, NiCuNi also shows magnetoresistance effect, and can affect therefore the performance of the method when used with magnets having NiCuNi coating. This paper studies the effects of PM coating on the performance magnetization estate estimation by means of high frequency signal using the magnetoresistance effect. The analysis will include NdFeB, AlNiCo and SmCo magnets. [1]**

***Index Terms*— High frequency signal injection, Magnetization State, Magnetoresistance, NiCuNi coating,**

I. Introduction

PMSMs have been widely studied and used during last decade due to their high efficiency, high power density and good dynamic response. However, the increased cost of rare earth materials during the last years has increased the interest in machine designs using less magnet materials, as well as on the substitution of rare earth materials by cheaper magnets (e.g. AlNiCo, Ferrite). However, these types of magnets can be demagnetized relatively easily, e.g. due to the temperature rise or the current injected in the stator windings under normal operation [1]. VF-PMSMs can either use low coercivity magnets, or combine high coercivity magnets (i.e. NdFeB) and low coercivity magnets (e.g. Ferrite, AlNiCo…) [2-4].

[1] This work was supported in part by Spanish Ministry of Education, Culture and Sports through "José Castillejo Program" under grant PX15/00354 and by Regional Ministry of Education, Culture and Sport of the Principality of Asturias through "Severo Ochoa Program" under Grant BP-13067.

VF-PMSMs magnetization state can be changed during normal operation of the machine by applying a current pulse to the stator terminals [3]. Knowledge of the magnetization state after a magnetization/demagnetization process is critical. Direct magnetization state estimation is not viable in practice, which has boosted the interest in the development of magnetization state estimation methods [5-7].

Magnetization state estimation methods can be divided into BEMF and high frequency signal injection based methods. BEMF based methods estimate the PM magnetization state from the PM flux linkage, which is obtained from the machine terminal voltages and currents [8], without interfering at all with the normal operation of the machine. These methods can be used in the mid-to-high speed region, but are not viable at very low/zero speed due to the reduced magnitude of the BEMF. In addition, previous knowledge of some machine parameters (i.e. stator resistance, inductance maps…) is needed. High frequency signal injection based methods can estimate the magnetization state either from the *d*-axis high frequency inductance [7], which changes with the saturation level, or from the stator reflected magnet high frequency resistance [5-6], which changes with the PM magnetization state due to the magnetoresistive effect [5]. Magnetoresistance based methods have been tested with NdFeB, Ferrite and SmCo magnets, NdFeB showing the highest sensitivity, SmCo and Ferrite showing very modest values [6].

PMs in PMSMs often use coating for protection, e.g. NdFeB magnets are usually protected to oxidation with NiCuNi coating. Previous studies have shown that coating can improve the magnetoresistance sensitivity in the machines equipped with Ferrite, AlNiCo or SmCo magnets [10-11]. However, this effect has not been studied in detail yet.

This paper analyses the effects of the PM coating on its magnetoresistance sensitivity. An experimental setup especially designed for this purpose will be used. The paper is organized as follows: Magnetoresistance effect is briefly reviewed in section II. High frequency signal injection for PM magnetization state estimation is presented in section III. Finally, experimental results are provided in section IV, while conclusions are presented in Section V.

II. Magnetoresistance Effect In Thin Film Layers

Magnetoresistance is defined in (1) as the change of the material electrical resistivity when an external magnetic field is

applied [9-10], where MR is the magnetoresistance, i.e. variation of resistivity due to the external field with respect to the initial resistivity, $\rho(0)$ is the resistivity of the material in the absence of magnetic field and $\rho(\mathrm{H})$ is the resistivity of the material and H the strength of the magnetic field being applied.

$$MR = \frac{\Delta\rho(\mathrm{H})}{\rho(0)} = \frac{\rho(\mathrm{H}) - \rho(0)}{\rho(0)} \quad (1)$$

The variation produced by the magnetoresistive effect over the absolute material resistance is defined by (2) where β is the coefficient that links the PM flux and the resistance variation (3).

$$R(\mathrm{H}) = R(\mathrm{H}_0)(1 + \beta(\mathrm{H} - \mathrm{H}_0)) \quad (2)$$

$$\beta = \frac{R(\mathrm{H}) - R(\mathrm{H}_0)}{(\mathrm{H} - \mathrm{H}_0)R(\mathrm{H}_0)} \quad (3)$$

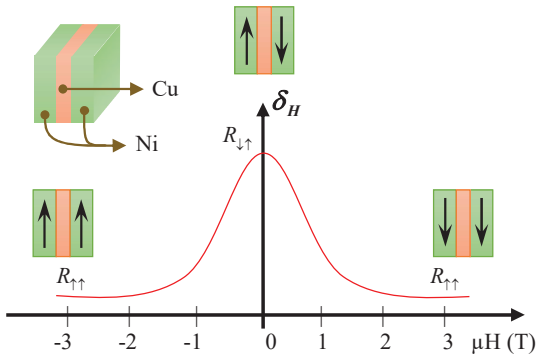

Fig.1 Magnetoresistance variations in multilayer structures.

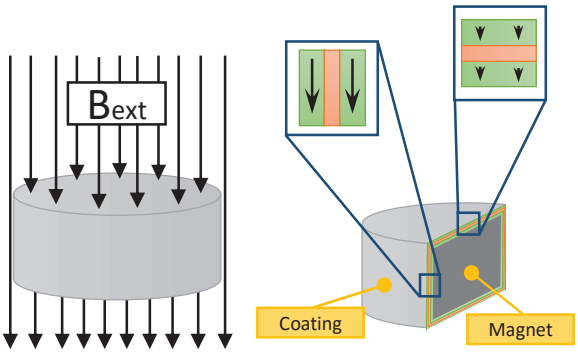

Fig.2 Magnetization direction of the coating layers when an external magnetic field is applied

Not all materials have the same sensitivity to the magnetoresistance effect. As already mentioned, NdFeB magnets have a higher sensitive compared to Ferrite and SmCo magnets [6]. In addition, certain designs, e.g. the layer stack arrangement shown in Fig. 1, can be used to increase the sensitivity to magnetoresistance effect in magnetoresistive sensors, the sensitivity increasing with the number of layers [10]. Giant magnetoresistance (GMR) is defined when the variation of the electrical resistance is higher than 10% [12]. A common arrangement to achieve GMR is a three-layer stack made of two ferromagnetic materials (e.g. Niquel, Iron…) and an electric conductor, non-ferromagnetic material (e.g. copper, gold…, see Fig. 1). The resistor model for GMRs is defined by (4) where $R_{\uparrow\downarrow}$ is the resistance with opposite magnetization in layers (i.e. in absence of $\underline{H}$), $R_{\uparrow\uparrow}$ is the resistance measured when the same direction of field H is applied to the layers and δ_H is the GMR [10]. Therefore β is function of both MR and δ_H (5).

$$\delta_H = \frac{\Delta R}{R(0)} = \frac{R_{\uparrow\uparrow} - R_{\uparrow\downarrow}}{R_{\uparrow\downarrow}} \quad (4)$$

$$\beta(\mathrm{H},\uparrow\uparrow,\uparrow\downarrow) = \frac{R(\mathrm{H},\uparrow\uparrow) - R(\mathrm{H}_0,\uparrow\downarrow)}{\Delta\mathrm{H}\,R(\mathrm{H}_0,\uparrow\downarrow)} \quad (5)$$

It is interesting to note the similarities between the arrangements shown in Fig. 1 to maximize the magnetoresistive effect in the magnetoresistive sensors and the NiCuNi coating used with NdFeB magnets to avoid oxidation (see Fig. 2).

III. Magnet High Frequency Resistance Measurement

The procedure used to measure the magnet high frequency resistance is presented in this section. The experimental setup that will be used is shown in Fig. 3. It consists of a magnetic core made of iron powder [5, 6] and a coil. The core was constructed using Fe-Si alloy iron powder blocks (BK8320-26 and CK2020-26, μ_r=26) [5, 6]. The core has a cylindrical shape central column, the magnet having the same diameter as the central column [5, 6].

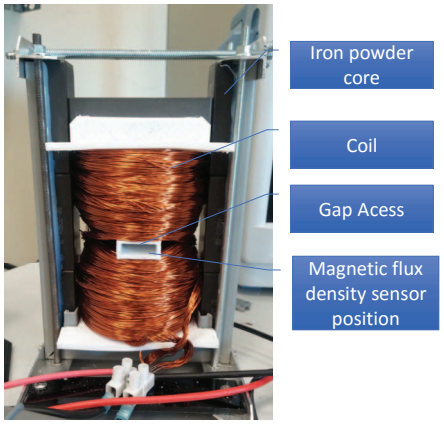

Fig. 3. Experimental setup used for PM magnetoresistance evaluation.

The coil in Fig. 3 is fed by an H-bridge (Fig. 4). The H-bridge allows simultaneous injection of both DC current used to change the PM sample magnetization state and the high frequency current used to estimate the magnet sample magnetization state. The system parameters are shown in Table I. Fig. 5 shows the power converter control block diagram. A PI controller is used to control the injected DC current i_{DCp}^{p*}, while a resonant controller is used to control the injected the high frequency current i_{hfp}^{p*}.

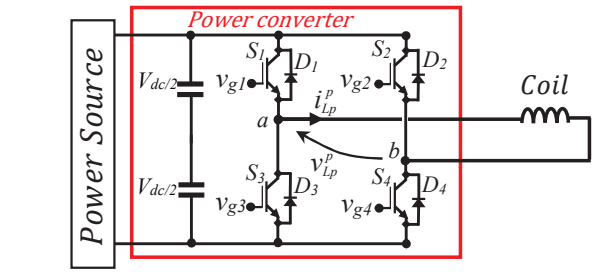

Fig. 4. H-Bridge powe converter

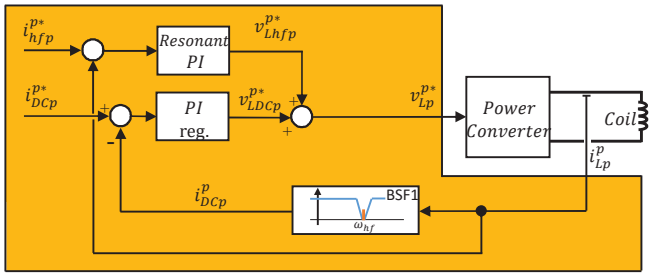

Fig.5. Block diagram of the DC and high frequency signal

TABLE I. EXPERIMENTAL SETUP PARAMETERS

Coil Parameters		Core Parameters		Single Phase Inverter Rated Parameters	
Number of turns	490	Central column diameter (mm)	20	Switching frequency	10 kHz
Resistance (Ω)	0.699 5	Saturation, B_{sat} (T)	1.6	Voltage	380 V
Parallel wires per turn	7	Relative permeability, μ_r	26	Current	75 A
Inductance (mH)	12.5			*BSF1*	10Hz
α_{cu} (1/K)	3.9e-3			Bandwidth of current reg.	200Hz

When the coil is fed with a high frequency current i^p_{hfp} (6), the overall high frequency impedance is given by (7), where v^p_{hfp} is the high frequency voltage, Z_{hfp} is the overall high frequency impedance, while R_{hfp} and L_{hfp} are the overall high frequency resistance and inductance respectively. The real part of the high frequency impedance, R_{hfp}, is a function of the coil R^p_{hfp}, core R^p_{hfFEp} and magnet R^p_{hfs} high frequency resistance.

$$i^p_{hfp} = I_{hf}\sin(\omega_{hf}\,t) \tag{6}$$

$$Z_{hfp} = \frac{v^p_{hfp}}{i^p_{hfp}} = \left(R_{hfp} + j\omega_{hf}L_{hfp}\right) = R_{hf} + j\omega_{hf}L_{hf} \tag{7}$$

$$R^p_{hfFEp} = R_{hfp} - R^p_{hfp} \tag{8}$$

$$R^p_{hfs} = \frac{R^p_{hfp}R^p_{hfFEp} - R_{hfp}R^p_{hfFEp}}{R_{hfp} - R^p_{hfp} - R^p_{hfFEp}} \tag{9}$$

The reflected magnet high frequency resistance, R^p_{hfs}, can be estimated from the overall coil high frequency resistance, R_{hfp}. However, this requires decoupling of the coil (R^p_{hfp}) and core (R^p_{hfFEp}) contributions to the overall high frequency resistance.

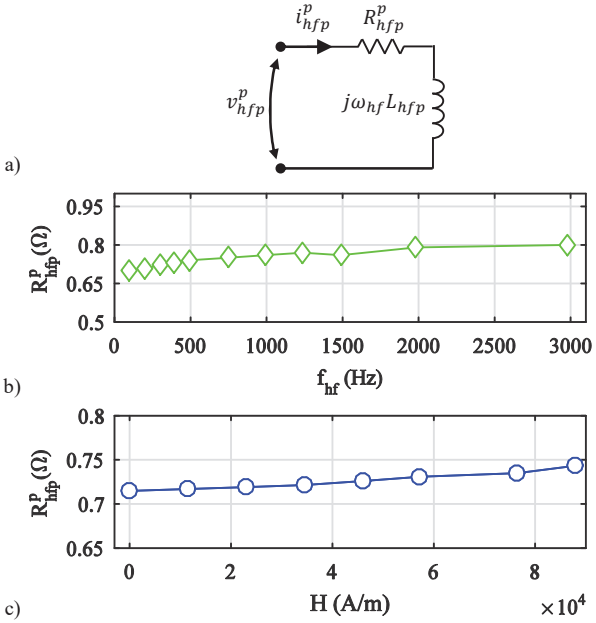

Fig. 6. a) Equivalent high frequency circuit of the experimental setup without core and magnet, b) coil high frequency resistance, R^p_{hfp}, for different frequencies, c) coil high frequency resistance, R^p_{hfp}, for different values of H values. f_{hf}=250Hz and I_{hf}=1A.

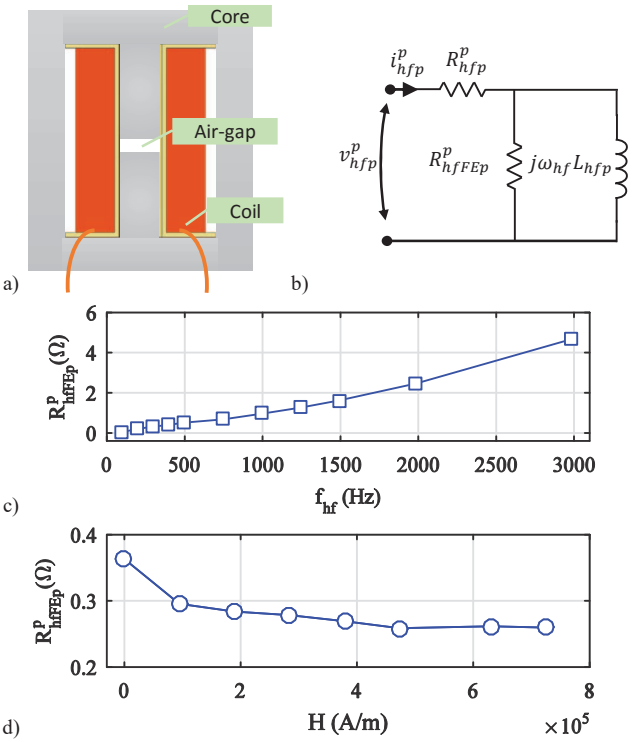

Fig. 7. a) Experimental setup configured for core high frequency resistance estimation (i.e. without magnet), b) equivalent high frequency circuit and c) core high frequency resistance for different frequency values, d) R^p_{hfp}, for different H values. f_{hf}=250Hz and I_{hf}=1A.

The coil high frequency resistance R^p_{hfp} can be approximated by removing the coil from the core and injecting a high frequency signal. Under these conditions, the equivalent high frequency circuit is shown in Fig. 6a. Figs. 6b shows R^p_{hfp} vs. the frequency of the injected signal. Fig. 6c show R^p_{hfp} vs. the strength of the magnetic field, H, which is

produced by forcing a DC current into the coil. As expected, R^p_{hfp} increases as the frequency does due to the skin effect (see Fig. 6b). Also as expected, R^p_{hfp} slightly increases with H, meaning that the magnetoresistive effect in the coil (made of copper) cannot be negligible

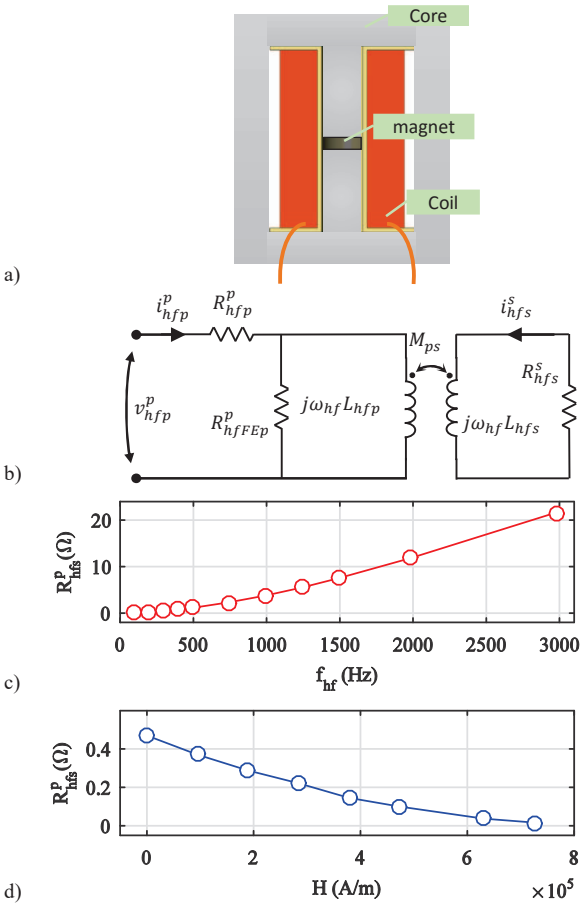

Fig. 8. a) Experimental setup configured for magnet high frequency resistance estimation, b) equivalent high frequency circuit, c) magnet high frequency resistance for different frequency values, d) R^p_{hfp}, for different H values. f_{hf}=250Hz and I_{hf}=1A.

The core high frequency resistance, i.e. R^p_{hfFEp}, can be estimated by injecting a high frequency signal into the coil with the coil and the core assembled, and replacing the magnet in the central column by a non-ferromagnetic material (see Fig. 7a). Fig. 7b shows the equivalent circuit in this case, the core high frequency resistance being obtained after decoupling the coil high frequency resistance, R^p_{hfp} (8). Figs. 7c and 7d show R^p_{hfFEp} vs. the frequency of the injected signal and vs. H, similar to Figs. 6b and 6c. As for R^p_{hfp}, R^p_{hfFEp} increases with frequency due to the skin effect (see Fig. 7c). It is observed from Fig. 7d that R^p_{hfFEp} decreases as H increases, meaning that core is slightly affected by the magnetoresistive effect. This was an expected result [6].

Finally, the contribution of the magnet resistance, R^p_{hfs}, to the overall high frequency resistance can be measured by inserting the magnet in the central column of the core (Fig. 8a), once the core and coil contribution to the overall high frequency resistances is decoupled (9). The equivalent circuit and measured high frequency resistance in this case are shown in Fig. 8b and Fig. 8c, for a NdFeB magnet. It is observed from this figure that R^p_{hfs} significantly decreases with H, i.e. the magnet is strongly affected by the magnetoresistive effect.

IV. Experimental Results

Experimental results measuring the effect of coating on the magnetoresistive effect using the experimental setup shown in Fig. 3 are presented in this section. Demagnetized and magnetized NdFeB, SmCo and AlNiCo disk shaped magnets have been tested. Two types of coatings, NiCuNi and Epoxy were used. Magnet thickness 5 and 10 mm, were selected. all with the same radius (see Fig. 9).

TABLE II. Experimental Setup Parameters

Coil Parameters		Single Phase Rated Parameters	
Number of Turns	335	Switching frequency (kHz)	10
Resistance (Ω)	0.3236	Voltage (V)	380
Inductance (mH)	5.2	Current (A)	75

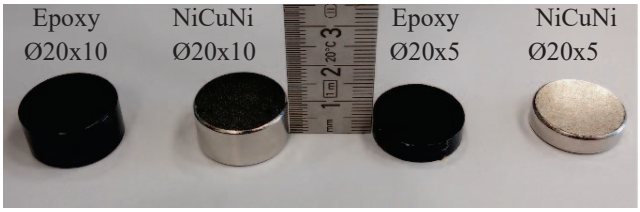

Fig. 9. Magnet shape, size and coating type evaluated for NdFeB, AlNiCo and SmCo.

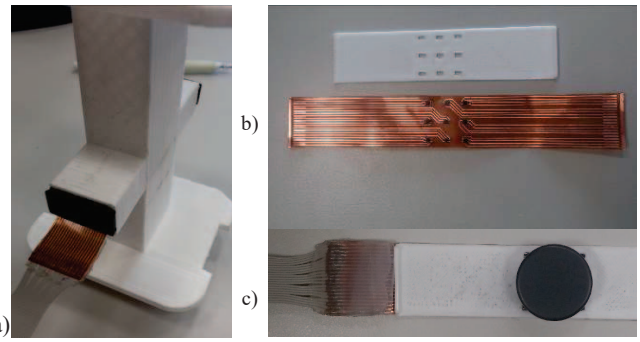

Fig. 10. Flux density sensor position, a) flux density sensor, b).position of the magnet on the sebsor array

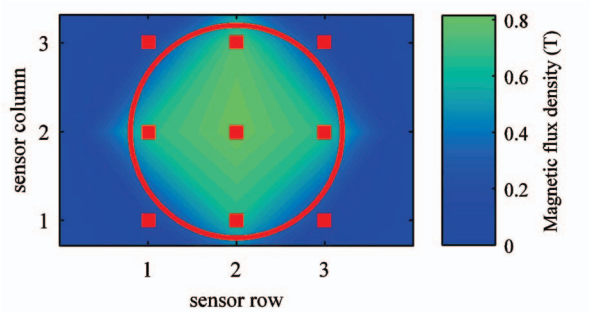

Fig11.Magnetic flux density distribution on magnet surface for a demagnetized NdFeB magnet when constant DC field is applied by the coil. Magnet location is indicated by the red circle, sensors location are represented by red squared spots.

Epoxy coating presents the same magnetic permeability as air. It was used to keep the same total magnet width, avoiding variations in the equivalent reluctance path of the prototype. In

addition, the thickness of the magnet material is also kept constant, avoiding errors due to the differences in volume among samples. Magnets and coating characteristics are summarized in Table III.

If magnetic flux density is measured with only one sensor, errors may occur as the magnetization is not uniform along the magnet surface [6]. To avoid this problem, a thin PCB (0.7mm thickness), see Fig. 10, that is equipped with a matrix of 3x3 Hall sensors was designed to measure the magnet flux density distribution on the magnet surface. The measurement provided by all the nine field sensors will be averaged, and used as a metric of the PM magnetic flux density. Fig. 10 shows an example of a contour plot of the field measured by the Hall sensor array when the magnet is fully demagnetized and a DC field of ≈0.8 T is applied by injecting a DC current into the coil terminals, see Fig. 8a.

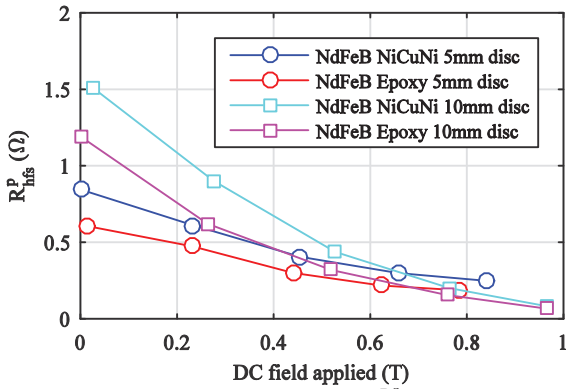

Fig. 12. Reflected high frequency resistance R^p_{hfs} of a NdFeB magnet with Epoxy coating, ○, and NiCuNi coating, □. 20ºC, f_{hf}=250Hz and I_{hf}=1A

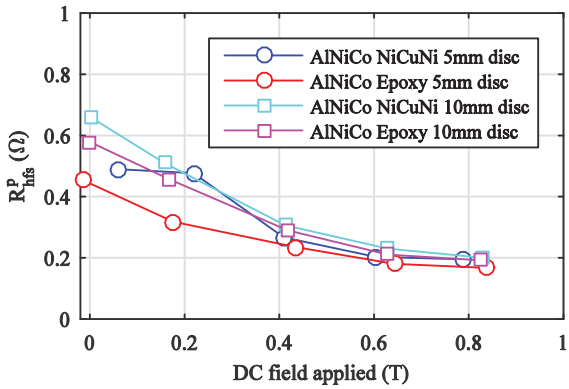

Fig. 13. Reflected high frequency resistance R^p_{hfs} of a AlniCo magnet. Same conditions as in Fig. 12

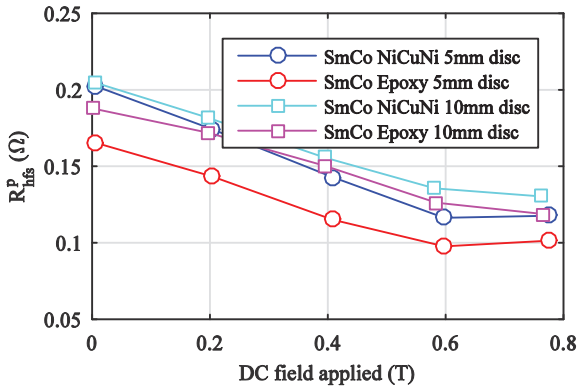

Fig. 14. Reflected high frequency resistance, R^p_{hfs} of an SmCo magnet. Same conditions as in Fig. 12.

TABLE III: MAGNETIC MATERIAL AND COATING THICKNESS

Materials	NdFeB (N42H)	SmCo (2:17)	AlNiCo
Ni layer thickness (μm)	3	3	3
Cu layer thickness (μm)	4	4	4
NiCuNi Coating Thickness (μm)	11	11	11
Epoxy thickness	6	6	6
Magnetic Material Thickness (mm)	5, 10	5, 10	5, 10

A. Demagnetized samples

Figs. 12-14 show the reflected magnet high frequency resistance, R^p_{hfs}, for the NdFeB, SmCo and AlNiCo samples. The demagnetized PMs are inserted in the core as shown in Fig. 8a. The magnet, coil and core temperatures are at room temperature. All magnets were initially fully demagnetized, B being therefore the result of the injected DC current. The high frequency current used for high frequency resistance estimation is superimposed to the DC current. The core and coil high frequency resistances are decoupled from the total estimated high frequency resistance (9), using the data shown in Figs. 6c and 7d.

It can be observed from Figs. 12-14 that the thicker magnets show larger high high frequency resistance when no DC field is applied. Most PMs materials show similar values of the estimated high frequency for large values of the DC field (>0.7T), independently of the magnet thickness. The exception is the SmCo magnet, see Fig. 14, magnet with epoxy coating, which shows slightly lower resistance at high DC magnetic fields. The highest variation of the high frequency resistance is observed for NdFeB magnets. This was expected as this material presents the largest high frequency resistance variations with the magnetization state.

B. Magnetized samples

Thicker lines in Figs 15-20 show experimental results for NdFeB, AlNiCo and SmCo magnets, with and without coating, for five different magnetization levels, i.e. remanent fluxes, of 0, 25, 50, 75 and 100% of its nominal value (1.2 T for NdFeB, 0.8 T for AlNiCo and 0.9 T for SmCo magnets).

The magnet samples were magnetized using a peak magnetizer shown in Fig 21. The magnetizer parameters are shown in Table IV. Once the samples are magnetized, they are inserted in the core shown in Fig 8a. No DC current is injected in this case, only the high frequency current signal needed for high frequency resistance estimation is being applied. The magnetic field shown in Figs. 15-20 is attributed therefore exclusively to the PM remanent flux.

It is observed that in all cases, the higher the magnetization state is, the lower is the reflected high frequency resistance. It is also observed that magnets with NiCuNi coating show larger high frequency resistance variations, meaning that they are

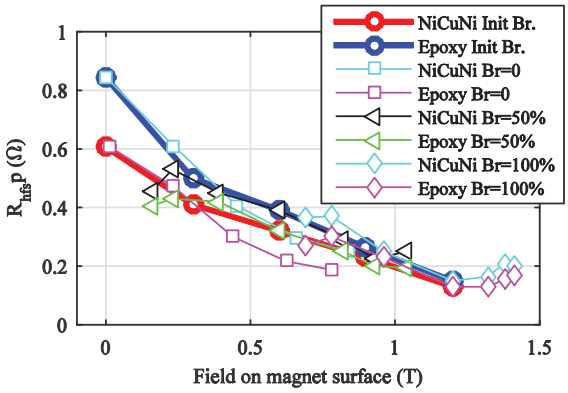

Fig. 15. Reflected PM magnet frequency resistance R_{hfs} for a 5mm thickness magnetized NdFeB magnet with epoxy, and NiCuNi coating, for different magnetization levels.

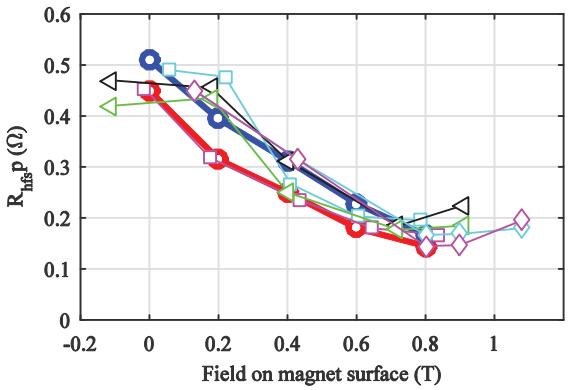

Fig. 16. Reflected PM magnet frequency resistance R_{hfs} for a 5mm magnetized AlNiCo magnet with epoxy, and NiCuNi coating, for different magnetization levels.

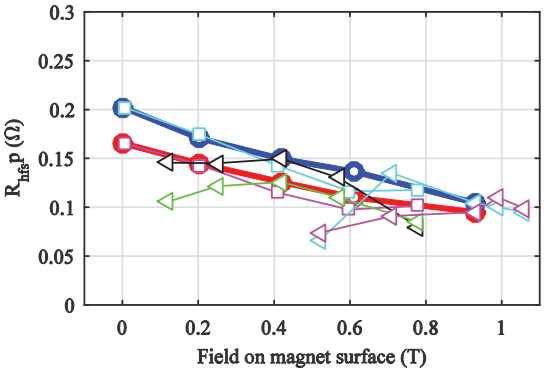

Fig. 17. Reflected PM magnet frequency resistance R_{hfs} for a 5 mm magnetized SmCo magnet with epoxy, and NiCuNi coating, for different magnetization levels.

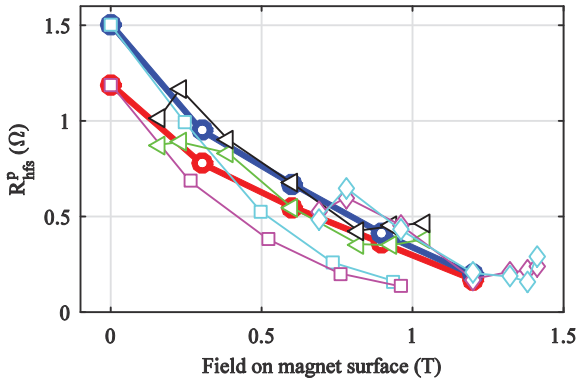

Fig. 18. Reflected PM magnet frequency resistance R_{hfs} for a 10 mm magnetized NdFeB magnet with epoxy, and NiCuNi coating, for different magnetization levels.

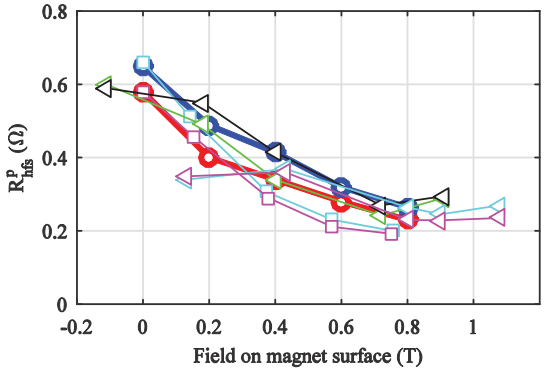

Fig. 19. Reflected PM magnet frequency resistance R_{hfs} for a 10 mm magnetized AlNiCo magnet with epoxy, and NiCuNi coating, for different magnetization levels.

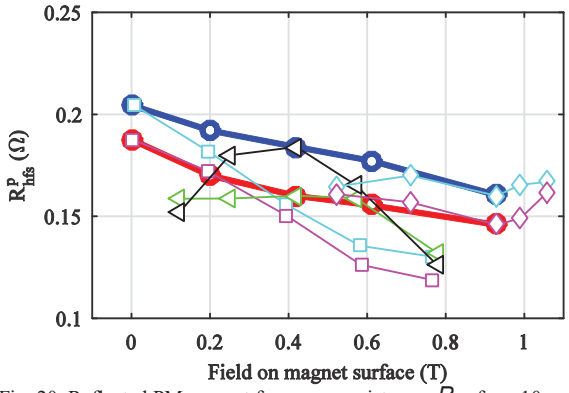

Fig. 20. Reflected PM magnet frequency resistance R_{hfs} for a 10 mm magnetized SmCo magnet with epoxy, and NiCuNi coating, for different magnetization levels.

more sensitive to the magnetoresistive effect. The estimated high frequency resistance when the magnetic field is produced externally by the coil (see Figs. 12-14) is different from the estimated high frequency resistance when the flux is produced by the magnet itself. This is mainly due to the differences in the magnetic flux distribution between magnetized magnet and demagnetized magnet within the magnetic circuit (see Figs 11 and 22).

C. Magnetoresistance in magnetized samples combined with flux-weakening and flux-intensifying current

Figs 15-20 show experimental results for NdFeB, AlniCo and SmCo magnets, with and without coating, for different magnetization levels, when flux weakening/ intensifying current is applied. Thicker lines show the high frequency resistance obtained for different DC current levels, for three different values of the initial magnetization level of ≈0, 50 and 100%. The maximum injected DC current is limited by the

power losses in the coil, as coil and magnet should remain at constant temperature for all the experiments. As in the previous cases, a high frequency signal is superposed to the DC current for high frequency resistance estimation.

For each initial magnetization level, the magnet flux is weakened or intensified by injecting a DC current. It is observed that in all cases the estimated resistance in absence of DC current increases when the permanent magnet flux is weakened and decreases as the magnetic field the magnet surface increases. Different trends are observed by the estimated high frequency resistance for different PM remanences and for magnetized magnets when an external field is used to weaken/intensify its field, no determinant conclusion is reached for this results.

It is concluded from the experimental results that the studied magnet materials coating changes the magnetoresistance effect. The largest high frequency resistance variations are for NdFeB, being slightly smaller for AlNiCo magnets. SmCo magnets show the smallest high frequency resistance variations.

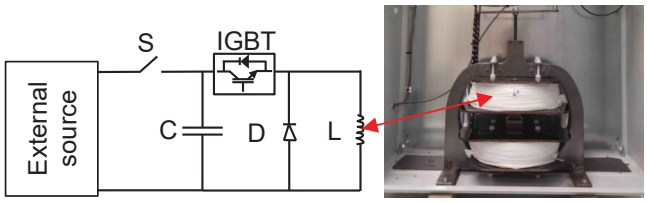

Fig. 21. Schematic representation of the circuit used for PM magnetization and demagnetization

TABLE IV. MAGNETIZATION CIRCUIT PARAMETERS

External source max. voltage	750 V
Capacitor "C"	11750 μF
Diode "D"	1000 V, 1250 A
IGBT	1700 V, 1400 A
Coil "L"	1960 turns

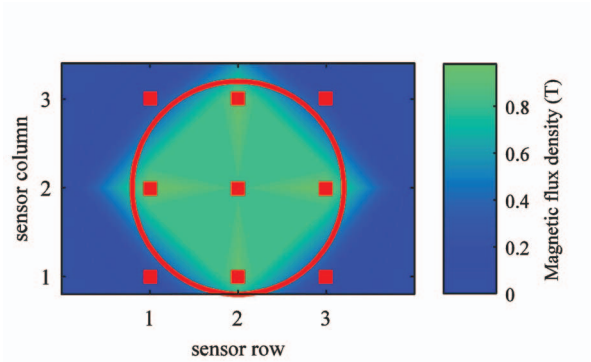

Fig. 22. Magnetic flux density distribution on magnet surface for a fully magnetized NdFeB. Magnet size and position is represented by the red circle,, sensors positions represented by red squared spots.

V. CONCLUSION

This paper presents an analysis of the contribution of the PM coating to magnetoresistance sensitivity. The physical principles of the proposed methodology for magnetization state estimation use the same principles as in GMR structures. Experimental results using NdFeB, SmCo and AlNiCo magnets with NiCuNi and epoxy coatings have been presented. It has been demonstrated the coating improves the magnetorresistive effect sensitivity, NdFeB showing the highest increments in sensitivity.

REFERENCES

[1]. N. Bianchi and T. M. Jahns "Design, analysis, and control of interior PM synchronous machines," Tutorial Course Notes, IEEE-IAS'04, Oct. 2004.

[2]. N. Limsuwan, T. Kato, K. Akatsu and R.D. Lorenz, "Design and evaluation of a variable-flux flux-intensifying interior permanent-magnet machine," IEEE Trans. on Ind. Appl., 50(2): 1015–1024, Nov.-Dec. 2014.

[3]. T. Fukushige, N. Limsuwan, T. Kato and R.D. Lorenz, "Efficiency contours and loss minimization over a driving cycle of a variable-flux flux-intensifying interior permanent magnet machine," IEEE-ECCE, pp. 591-597, Sept. 2013.

[4]. T. Fukushige, N. Limsuwan, T. Kato and R.D. Lorenz, "Electromagnetic performance analysis of a new stator-permanent-magnet doubly salient flux memory motor using a piecewise-linear hysteresis model," IEEE Trans. on Magnetics., 47(5): 1106–1109, May. 2011.

[5]. D. Reigosa, D. Fernandez, Z.Q. Zhu, F. Briz, "PMSM magnetization state estimation based on stator-reflected pm resistance using high frequency signal injection," IEEE Trans. on Ind. Appl., 51(5): 3800–3810, Sept.-Oct. 2015.

[6]. D. Fernandez, D. Reigosa, Guerrero, J.M., Z.Q. Zhu, F. Briz, " Permanent magnet magnetization state estimation using high frequency signal injection," IEEE-ECCE, pp. 3949-3956, Sept. 2015.

[7]. C. Y. Yu, T. Fukushige, A. Athavale, B. Gagas, K. Akatsu, D. Reigosa, R. D. Lorenz ,"Zero/low speed magnet magnetization state estimation using high frequency injection for a fractional slot variable flux-intensifying interior permanent magnet synchronous machine ," IEEE-ECCE, pp. 2495-2502, Setp. 2014.

[8]. M.F. Hsieh, D. G. Dorrell, C. K. Lin, P. T. Chen, and Peter Y. P. Wung, "Modeling and effects of in situ magnetization of isotropic ferrite magnet motors," IEEE Trans. on Ind. Appl., 50(1):364-374, Jan. 2014.

[9]. S. O. Kasap, "Principles of electronic materials and devices," Third Edition 2006, ISBN 0-07-295791-3.

[10]. Uwe Hartmann, "Magnetic Multilayers and Giant Magnetoresistance," First Edition 2000, ISBN 978-3-642-08487-4.

[11]. H. Kubota, M. Sato and T. Miyazaki, "Anomalous temperature dependence of giant magnetoresistance in Ni/Cu, Ni_{95}/Co_5 and $Ni_{95}Fe_5Cu$ multilayer films" Elsevier, Journal of Magnetism and Magnetic Materials. 167: 12–20, Apr. 1997.

[12]. B. Idzikowski, M. Wolf, A. Handstein, K. Nenkov, F. Stobieski and K.-H. Muller, "Inverse giant magnetoresistance in granular Nd/sub 2/Fe/sub 14/ B a-Fe," INTERMAG Magnetics Conference, Oct. 1997.